

# Quasistellar Objects: Intervening Absorption Lines<sup>1</sup>

Jane C. Charlton and Christopher W. Churchill  
*The Pennsylvania State University, University Park,  
 PA 16802*

## Abstract

We briefly review, at a level appropriate for graduate students and non-specialists, the field of quasar absorption lines (QALs). Emphasis is on the intervening absorbers. We present the anatomy of a quasar spectrum due to various classes of intervening absorption systems, and a brief historical review of each absorber class (Lyman-alpha forest and Lyman limit systems, and metal-line and damped Lyman-alpha absorbers). We also provide several heuristic examples on how the physical properties of both the intergalactic medium and the gaseous environments associated with earlier epoch galaxies can be inferred from QALs. The evolution of these environments from  $z=4$  are discussed.

## 1. Introduction

Every parcel of gas along the line of sight to a distant quasar will selectively absorb certain wavelengths of continuum light of the quasar due to the presence of the various chemical elements in the gas. Through the analysis of these quasar absorption lines we can study the spatial distributions, motions, chemical enrichment, and ionization histories of gaseous structures from redshift five until the present. This includes the gas in galaxies of all morphological types as well as the diffuse gas in the intergalactic medium.

### 1.1. Basics of Quasar Spectra

Figure 1 illustrates many of the common features of a quasar spectrum. The relatively flat

quasar continuum and broad emission features are produced by the quasar itself (near the black hole and its accretion disk). In some cases, gas near the quasar central engine also produces “intrinsic” absorption lines, most notably  $\text{Ly}\alpha$ , and relatively high ionization metal transitions such as C IV, N V, and O VI. These intrinsic absorption lines can be broad [thousands or even tens of thousands of  $\text{km s}^{-1}$  in which case the quasar is called a broad absorption line (BAL) QSO], or narrow (tens to hundreds of  $\text{km s}^{-1}$ ). However, the vast majority of absorption lines in a typical quasar spectrum are “intervening”, produced by gas unrelated to the quasar that is located along the line of sight between the quasar and the Earth.

A structure along the line of sight to the quasar can be described by its neutral Hydrogen column density,  $N(\text{HI})$ , the number of atoms per  $\text{cm}^2$ .  $N(\text{HI})$  is given by the product of the density of the material and the pathlength along the line of sight through the gas. Each structure will produce an absorption line in the quasar spectrum at a wavelength of  $\lambda_{obs} = \lambda_{rest}(1 + z_{abs})$ , where  $z_{abs}$  is the redshift of the absorbing gas and  $\lambda_{rest} = 1215.67 \text{ \AA}$  is the rest wavelength of the  $\text{Ly}\alpha$  transition. Since  $z_{abs} < z_{QSO}$ , the redshift of the quasar, these  $\text{Ly}\alpha$  absorption lines form a “forest” at wavelengths blueward of the  $\text{Ly}\alpha$  emission. The region redward of the  $\text{Ly}\alpha$  emission will be populated only by absorption through other chemical transitions with longer  $\lambda_{rest}$ . Historically, absorption systems with  $N(\text{HI}) < 10^{17.2} \text{ cm}^{-2}$  have been called  $\text{Ly}\alpha$  forest lines, those with  $10^{17.2} < N(\text{HI}) < 10^{20.3} \text{ cm}^{-2}$  are Lyman limit systems, and those with  $N(\text{HI}) > 10^{20.3} \text{ cm}^{-2}$  are damped  $\text{Ly}\alpha$  systems. The number of systems per unit redshift increases dramatically with decreasing column density, as illustrated in the schematic diagram in Figure 2. Lyman limit systems are defined by a sharp break in the spectrum due to absorption of photons capable of ionizing H I, i.e. those with energies greater than 13.6 eV. The optical

<sup>1</sup>Written for the Encyclopedia of Astronomy and Astrophysics (to be published in 2000 by MacMillan and the Institute of Physics Publishing)

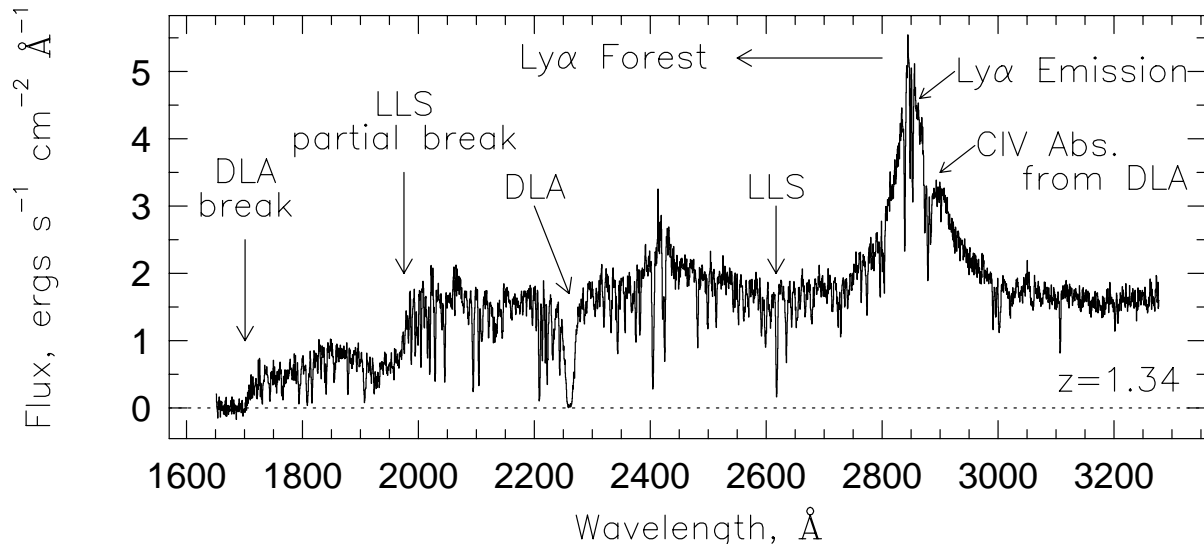


Fig. 1.— Typical spectrum of a quasar, showing the quasar continuum and emission lines, and the absorption lines produced by galaxies and intergalactic material that lie between the quasar and the observer. This spectrum of the  $z = 1.34$  quasar PKS0454 + 039 was obtained with the Faint Object Spectrograph on the Hubble Space Telescope. The emission lines at  $\sim 2400 \text{ \AA}$  and  $\sim 2850 \text{ \AA}$  are  $\text{Ly}\beta$  and  $\text{Ly}\alpha$ . The  $\text{Ly}\alpha$  forest, absorption produced by various intergalactic clouds, is apparent at wavelengths blueward of the  $\text{Ly}\alpha$  emission line. The two strongest absorbers, due to galaxies, are a damped  $\text{Ly}\alpha$  absorber at  $z = 0.86$  and a Lyman limit system at  $z = 1.15$ . The former produces a Lyman limit break at  $\sim 1700 \text{ \AA}$  and the latter a partial Lyman limit break at  $\sim 1950 \text{ \AA}$  since the neutral Hydrogen column density is not large enough for it to absorb all ionizing photons. Many absorption lines are produced by the DLA at  $z = 0.86$  (CIV  $\lambda\lambda 1548, 1550$ , for example, is redshifted onto the red wing of the quasar’s  $\text{Ly}\alpha$  emission line).

depth,  $\tau$ , of the break is given by the product  $N(\text{HI})\sigma$ , where the cross section for ionization of Hydrogen,  $\sigma = 6.3 \times 10^{-18} (E_\gamma/13.6 \text{ eV})^{-3} \text{ cm}^2$ , (and the flux is reduced by the factor  $e^{-\tau}$ ). The energy dependence of  $\sigma$  leads to a recovery of the Lyman limit break at higher energies (shorter wavelengths), unless  $N(\text{HI}) \gg 10^{17.2} \text{ cm}^{-2}$  (see Figure 1).

The curve of growth describes the relationship between the equivalent width of an absorption line,  $W$ , (the integral of the normalized profile) and its column density,  $N$ . Figure 3 shows that for small  $N(\text{HI})$  the number of absorbed photons, and therefore the flux removed, increases in direct proportion to the number of atoms. This is called the linear part of the curve of growth. As  $N$  is increased the line saturates so that photons are only absorbed in the wings of

the lines; in this regime the equivalent width is sensitive to the amount of line broadening (characterized by the Doppler parameter  $b$ ), but does not depend very strongly on  $N(\text{HI})$ . This is the flat part of the curve of growth. Finally, at  $N(\text{HI}) > 10^{20.3} \text{ cm}^{-2}$ , there are enough atoms that the damping wings of the line become populated and the equivalent width increases as the square root of  $N(\text{HI})$ , and is no longer sensitive to  $b$ .

In addition to the  $\text{Ly}\alpha$  ( $1s \rightarrow 2p$ ) and higher order ( $1s \rightarrow np$ ) Lyman series lines, quasar spectra also show absorption due to different ionization states of the various species of metals. Figure 1 illustrates that the damped  $\text{Ly}\alpha$  system at  $z = 0.86$  that is responsible for the  $\text{Ly}\alpha$  absorption line at  $\lambda_{obs} = 2260 \text{ \AA}$  and a Lyman limit break at  $\lambda_{obs} = 1700 \text{ \AA}$  also produces absorp-

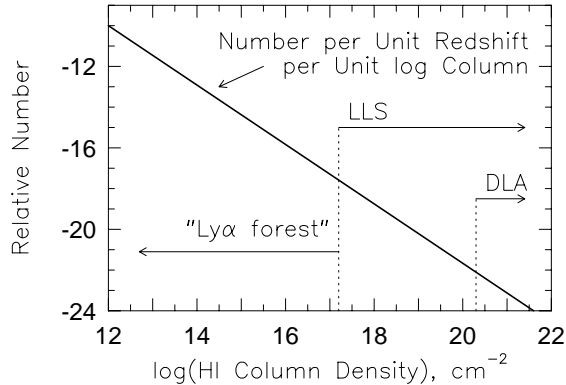


Fig. 2.— The column density distribution of Ly $\alpha$  clouds,  $f(N(\text{HI}))$ , roughly follows a power law over ten orders of magnitude; there are many more weak lines than strong lines. The column density regions for the three categories of systems are shown: Ly $\alpha$  forest, Lyman limit, and damped Ly $\alpha$ . The term “Ly $\alpha$  forest” has at times been used to refer to metal-free Hydrogen clouds, perhaps those with  $N(\text{HI}) < 10^{16} \text{ cm}^{-2}$ , but now metals have been found associated with weaker systems down to the detection limit.

tion at  $\lambda_{obs} = 2870 \text{ \AA}$  due to the presence of CIV in the absorbing gas at that same redshift. Like many of the strongest metal lines seen in quasar spectra, CIV is a resonant doublet transition due to transitions from  $^2S_{1/2}$  energy levels to the  $^2P_{1/2}$  and to the  $^2P_{3/2}$  energy levels. (The left superscript “2” represents the number of orientations of the electron spin, the letter  $S$  or  $P$  represents the total orbital angular momentum,  $L$ , and the right subscript represents the total angular momentum,  $J$ .) Doublet transitions are easy to identify. The dichotomy between rest wavelength and redshift is resolved because the observed wavelength separation of the doublet members increases as  $1 + z$ .

Table 1 lists some of the metal lines that are commonly detected for intervening absorption systems. Many of these are only strong enough to be observable for quasar lines of sight that pass through the higher  $N(\text{HI})$  regions of galaxies.

Table 1: Common Transitions

Transition	$\lambda_{rest} [\text{\AA}]$
LL .....	$\sim 912$
Ly $\gamma$ .....	972.537
Ly $\beta$ .....	1025.722
Ly $\alpha$ .....	1215.670
SiIV 1393 .....	1393.755
SiIV 1402 .....	1402.770
CIV 1548 .....	1548.195
CIV 1550 .....	1550.770
FeII 2382 .....	2382.765
FeII 2600 .....	2600.173
MgII 2796 .....	2796.352
MgII 2803 .....	2803.531

## 2. History, Surveys, and Revolutionary Progress in the 1990’s

The history of quasar absorption lines began within a couple of years of the identification of the first quasar in 1963. In 1965, Gunn and Peterson considered the detection of flux blueward of the Ly $\alpha$  emission line in the quasar 3C 9, observed by Schmidt, and derived a limit on the amount of neutral Hydrogen that could be present in intergalactic space. In that same year, Bahcall and Salpeter predicted that intervening material should produce observable discrete absorption features in quasar spectra. Such features were detected in 1967 in the quasar PKS 0237 – 23 by Greenstein and Schmidt, and in 1968 in PHL 938 by Burbidge, Lynds, and Stockton. By 1969 many intervening systems had been discovered, and Bahcall and Spitzer proposed that most with metals were produced by the halos of normal galaxies. As more data accumulated, the sheer number of Ly $\alpha$  forest lines strongly supported the idea that galactic and intergalactic gas, and not only material intrinsic to the quasar, is the source of most quasar absorption lines.

In the 1980’s many more quasar spectra were

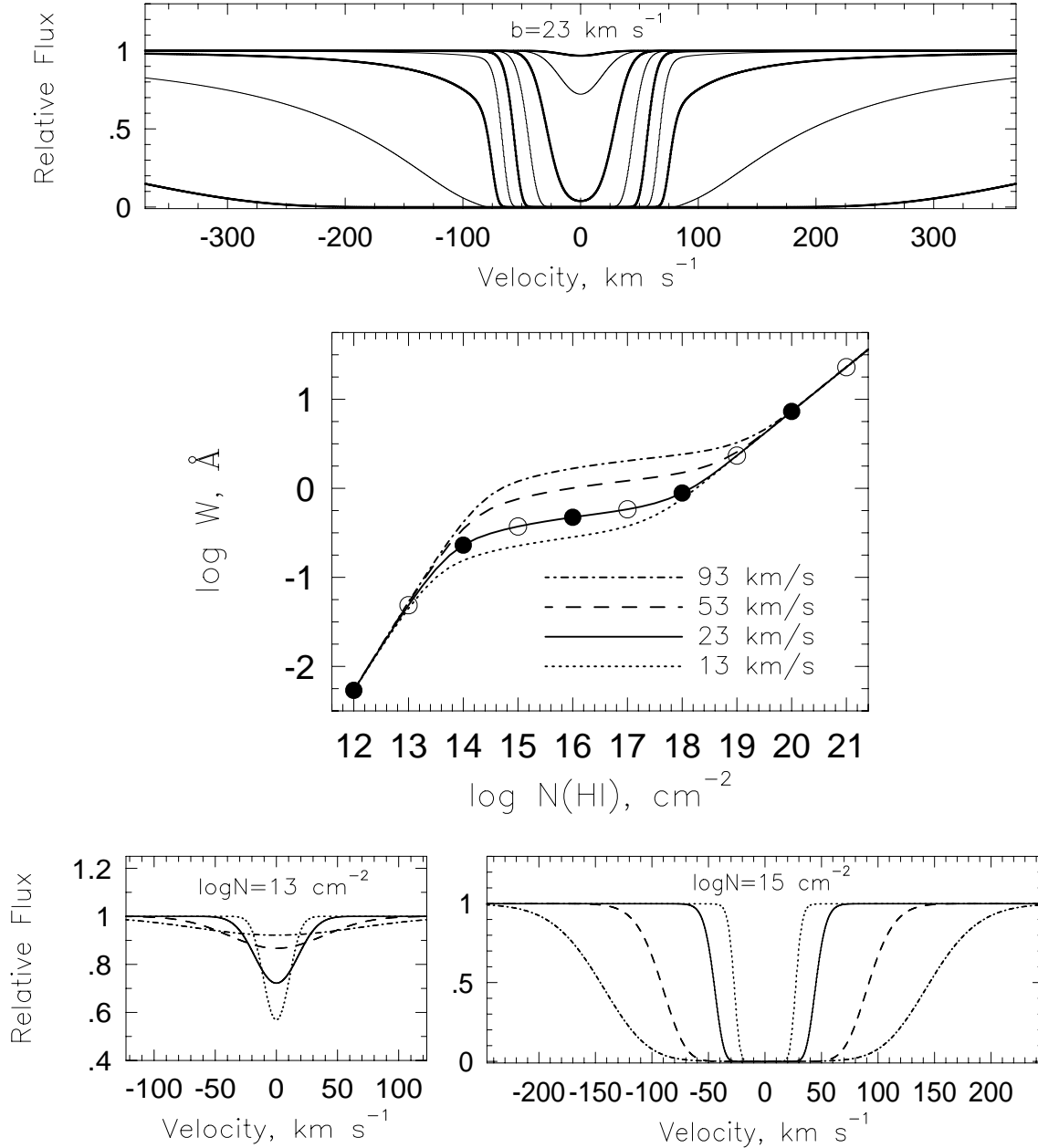


Fig. 3.— Illustration of the different regimes of the curve of growth. The middle panel shows the curve of growth for the Ly $\alpha$  transition, relating the equivalent width,  $W$ , of the absorption profile to the column density,  $N(\text{HI})$ . The different curves represent four different values of the Doppler parameter:  $b = 13, 23, 53,$  and  $93 \text{ km s}^{-1}$ . The upper panel shows absorption profiles with Doppler parameter  $b = 23 \text{ km s}^{-1}$  for the series of neutral hydrogen column densities  $N(\text{HI}) = 10^{12} - 10^{20} \text{ cm}^{-2}$ . The thick (thin) curves correspond to the filled (open) points on the  $b = 23 \text{ km s}^{-1}$  curve of growth (middle panel), starting at  $N(\text{HI}) = 10^{12} \text{ cm}^{-2}$ . For  $N(\text{HI}) < 10^{13} \text{ cm}^{-2}$ , known as the linear part of the curve of growth, the equivalent width does not depend on  $b$ . The lower left panel shows that, at fixed  $N(\text{HI})$ , the depth of the profile is smaller for large  $b$ , such that the equivalent width remains constant. On the flat part of the curve of growth, profiles are saturated and the equivalent width increases with  $b$  for constant  $N(\text{HI})$ . For  $N(\text{HI}) > 10^{20} \text{ cm}^{-2}$ , the profile develops damping wings, which dominate the equivalent width.

obtained and many large statistical surveys of the different classes of absorption line systems were published. The emphasis was to characterize the number of lines per unit redshift,  $dN/dz$ , stronger than some specified equivalent width limit. With 4m-class telescopes [equipped with charge coupled device (CCD) detectors] it was possible to conduct surveys with a spectral resolution of  $R \sim 1000$ . The spectral resolution is defined as  $R = \lambda/\Delta\lambda = c/\Delta v$ , so that  $R = 1000$  corresponds to  $300 \text{ km s}^{-1}$  or  $5 \text{ \AA}$  at  $\lambda = 5000 \text{ \AA}$ . Separate surveys were conducted for Ly $\alpha$  lines, MgII doublets, CIV doublets, and also for Lyman limit breaks, all as a function of redshift. The Ly $\alpha$  line is observable in the optical part of the spectrum for  $z > 2.2$ , MgII for  $0.4 < z < 2.2$ , CIV for  $1.7 < z < 5.0$ , and the Lyman limit break for  $z > 3$ . However, a break is also easily identified in lower resolution space-based UV spectra, which extended Lyman limit surveys to lower redshift.

In order to consider the cross section of the sky covered by the different populations, it can be assumed that absorption will be observed for all lines of sight within some radius of every luminous galaxy ( $> 0.05L_K^*$ ). ( $L_K^*$  represents the Schechter luminosity, i.e. the transition between the exponential and the power law forms of the luminosity function, and corresponds to a  $K$ -band absolute magnitude of  $M_K = -25$ ). To explain the observed  $dN/dz$  at  $z \sim 1.5$ , this radius would be 70 kpc for strong CIV (detection sensitivity  $0.4 \text{ \AA}$ ), and 40 kpc for strong MgII (detection sensitivity  $0.3 \text{ \AA}$ ) and also for Lyman limit systems, implying that the latter two populations are in fact produced in the same gas. The higher  $N(\text{HI})$  damped Ly $\alpha$  absorbers would be produced within 15 kpc of the center of each galaxy, while the Ly $\alpha$  forest lines would require a considerably larger region, hundreds of kpcs around each galaxy to produce a cross section consistent with the observed number of weak lines.

Up until the 1990's, the focus of quasar ab-

sorption line work was to separately consider the properties of the individual classes of absorbers (eg. Ly $\alpha$  forest or MgII absorbers). In the 1990's, however, three different observational advances led to recognition of the direct connections between the different classes of quasar absorption lines, and of direct associations with the population of galaxies:

1. Deep images of quasar fields could be obtained, and redshifts of the galaxies in the field could be determined from low resolution spectra. Steidel found that whenever MgII absorption with  $W_r(\text{MgII}) > 0.3 \text{ \AA}$  is observed, a luminous galaxy ( $L_K > 0.06L_K^*$ ) is found within an impact parameter of  $38h^{-1}(L/L_K^*)^{-0.15} \text{ kpc}$  with a redshift coincident with that determined from the absorption lines. Also, it is rare to find a galaxy within this impact parameter that does not produce MgII absorption. There appears to be a one-to-one correspondence between strong MgII absorption and luminous galaxies. The MgII absorbing galaxies span a range of morphological types.

2. The High Resolution Spectrograph on the Keck I 10-meter telescope made it possible to obtain quasar spectra at a resolution of  $R = 45,000$ , which corresponds to  $\sim 6 \text{ km s}^{-1}$ . The previous surveys with resolution of order hundreds of  $\text{km s}^{-1}$  identified absorption due to entire galaxies and their environments. With  $6 \text{ km s}^{-1}$  resolution it became possible to resolve structure within a galaxy: the clouds in its halo, the interstellar medium of its disk, and the satellites and infalling gas clouds in its environment. Figure 4 is a dramatic illustration of this contrast for the MgII absorber at  $z = 0.93$  toward the quasar PG 1206 + 459.

3. The Faint Object Spectrograph (FOS) on the Hubble Space Telescope provided resolution  $R \sim 1000$  in the UV, from 1400–3300  $\text{\AA}$ . Observations of Ly $\alpha$  forest clouds could be extended from  $z = 2.2$  down to the present epoch. Furthermore, absorption from a given galaxy could be observed in numerous transitions; if MgII was

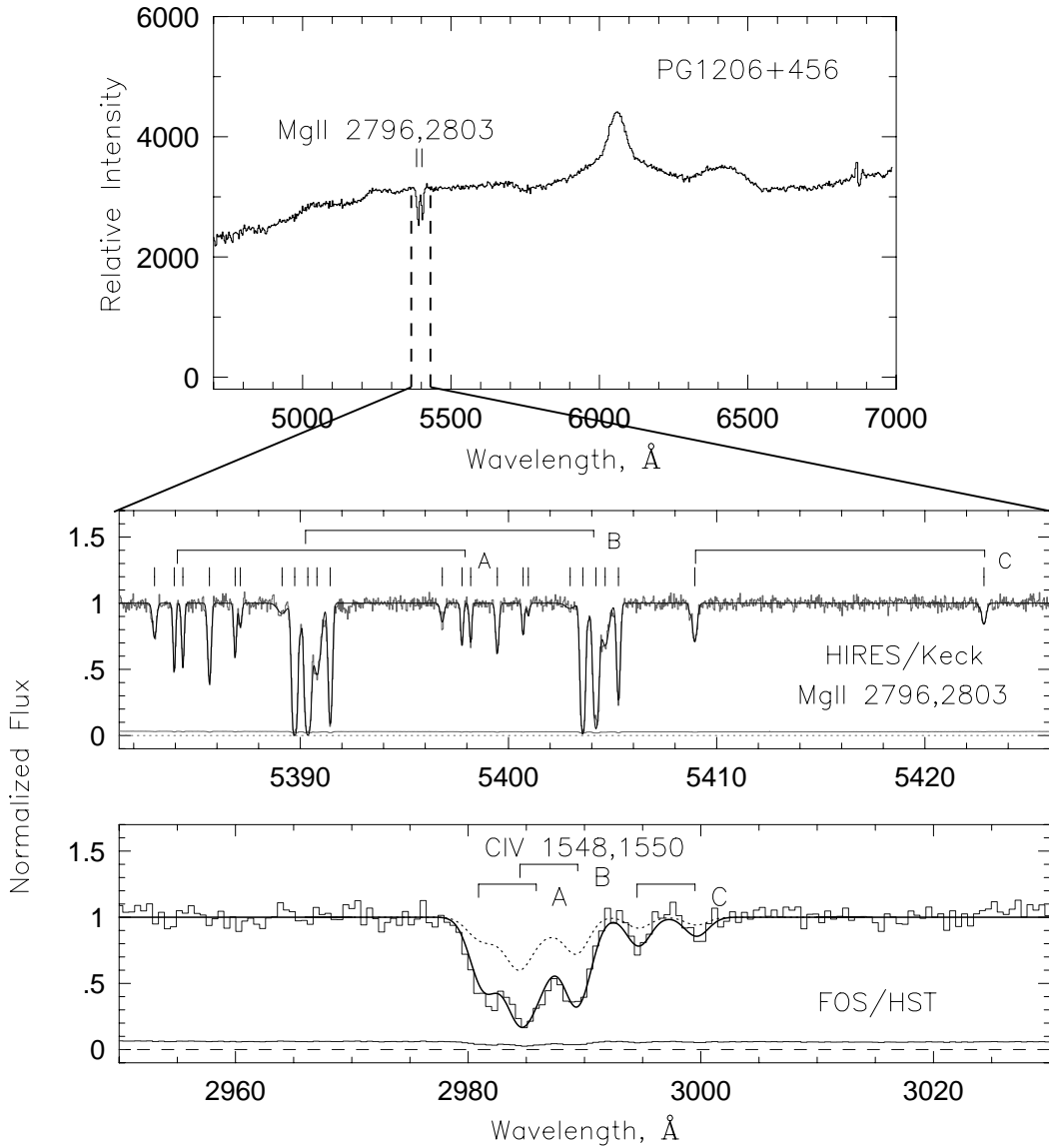


Fig. 4.— Dramatic demonstration of gains due to high resolution spectroscopy of the MgII doublet. The top panel is a  $R = 3000$  spectrum of PG1206 + 459. The doublet that is apparent at an observed wavelength of  $\sim 5400$  Å is due to MgII absorption from a system at  $z = 0.927$ . The middle panel shows the remarkable kinematic structure that is revealed at the resolution ( $R = 45,000$ ) of the Keck/HIRES spectrograph of the same quasar. The 2796 Å transition is resolved into multiple components (5583–5592 Å), which also appear in the 2803 Å transition (5396–5406 Å). This system can be separated in two “clusters” of clouds, labeled “A” and “B”. Another weaker MgII doublet is observed at 5409 and 5423 Å, from a system at  $z = 0.934$  Å, labeled with a “C”. The solid line through these complex MgII profiles is the result of multiple Voigt profile fitting, with a cloud centered on each of the ticks drawn above the spectrum. The lower panel shows the CIV doublets associated with the same three systems, observed with the Faint Object Spectrograph on HST, but at much lower resolution ( $R = 1300$ ). The CIV is in three different concentrations around the three systems “A”, “B”, and “C”. The CIV $\lambda$ 1550 transition from system A is blended with the CIV $\lambda$ 1548 transition from system B. The CIV equivalent width is too large for this absorption to be produced by the same phase of gas that produces the MgII cloud absorption. The maximum absorption that can arise in the MgII phase is given by the dotted line; a plausible model with a kinematically broader CIV phase yields the solid curve.

observed in the optical, the Lyman series and CIV could be studied in the UV (see Figure 4). With information on transitions with a range of ionization states, consideration of the degree of ionization (related to the gas density and the intensity and shape of the ionizing radiation field) and the multiple phase structure of galactic gas became possible.

No longer is analysis of absorption lines in quasar spectra an esoteric subject. It has developed into a powerful tool to be used in the study of galaxy evolution (eg. similar to imaging the stellar components of the galaxies). At least in principle, quasar spectra can be used for an unbiased study of the gaseous environments of galaxies from the present back to the highest redshifts at which quasars are observed. Gas structures smaller than  $1 M_{\odot}$  can be detected if they are intercepted by the quasar line of sight, irrespective of whether they emit light. Through the tool of quasar absorption lines, proto-galactic structures and low surface brightness galaxies can be studied as well as high luminosity galaxies.

### 3. Developing Physical Intuition

With high resolution spectra of quasars, it is possible to consider the physical conditions of the gaseous structures that produce absorption. However, it is challenging to separate the various effects that “shape” the spectral features in the different chemical transitions. The absorption profiles observed for the different chemical transitions are determined by a combination of the spatial distribution of material along the line of sight, its bulk kinematics, temperature, metallicity, and abundance pattern. The ionization structure is influenced by gas densities and by the UV radiation field, which is a combination of the extragalactic background radiation due to the accumulated effect of quasars and stellar photons escaped from galaxies (and corrected for absorption by the intergalactic medium).

The shape of an absorption line can be mod-

eled with a Voigt profile, which is a combination of the natural, quantum mechanical Lorentzian broadening and the Gaussian broadening caused by the thermal and turbulent motions in the gas. Several Voigt profiles can be blended together to form an overall complex absorption feature (see Figure 4). The “width” of a single Voigt profile is characterized by the Doppler parameter,  $b$  (expressed in velocity units and related to the Gaussian  $\sigma$  by  $b = 2^{1/2}\sigma$ ). Physically, the Doppler parameter is the sum of thermal and turbulent components,  $b_{tot}^2 = 2kT/m + b_{turb}^2$ , where  $T$  is the temperature of the gas, and  $m$  is the mass of an atom.

#### 3.1. Kinematic Models

Two of the simplest types of organized kinematics in galaxies are illustrated in Figure 5: clouds distributed in a rotating disk, and radial infall of clouds in a spherical distribution. Here, MgII absorbers are used as an example, but the same kinematic arguments would apply to other transitions. For radial infall, clouds can be distributed over the range of velocities, with a tendency for a “double peak” from material that is redshifted and blueshifted but with a considerable amount of variation if there are typically several discrete clouds along the line of sight. A rotating disk with a vertical velocity dispersion characteristic of a spiral galaxy disk ( $10\text{--}20 \text{ km s}^{-1}$ ) will have clouds superimposed in velocity space, and an overall kinematic spread of tens of  $\text{km s}^{-1}$ . Strong MgII absorption has been found to arise along nearly all lines of within  $\sim 40 \text{ kpc}$  of normal galaxies (i.e. the covering factor is nearly unity within that radius). The large variety of kinematics evident in MgII absorption profiles is, in fact, consistent with a superposition of disk and radial infall (halo) motions, and not with just one or the other. In addition to these simple, toy models, insights can be gleaned by passing lines of sight through the structures in cosmological N-body/hydrodynamic simulations. In a few studies, metals have been added

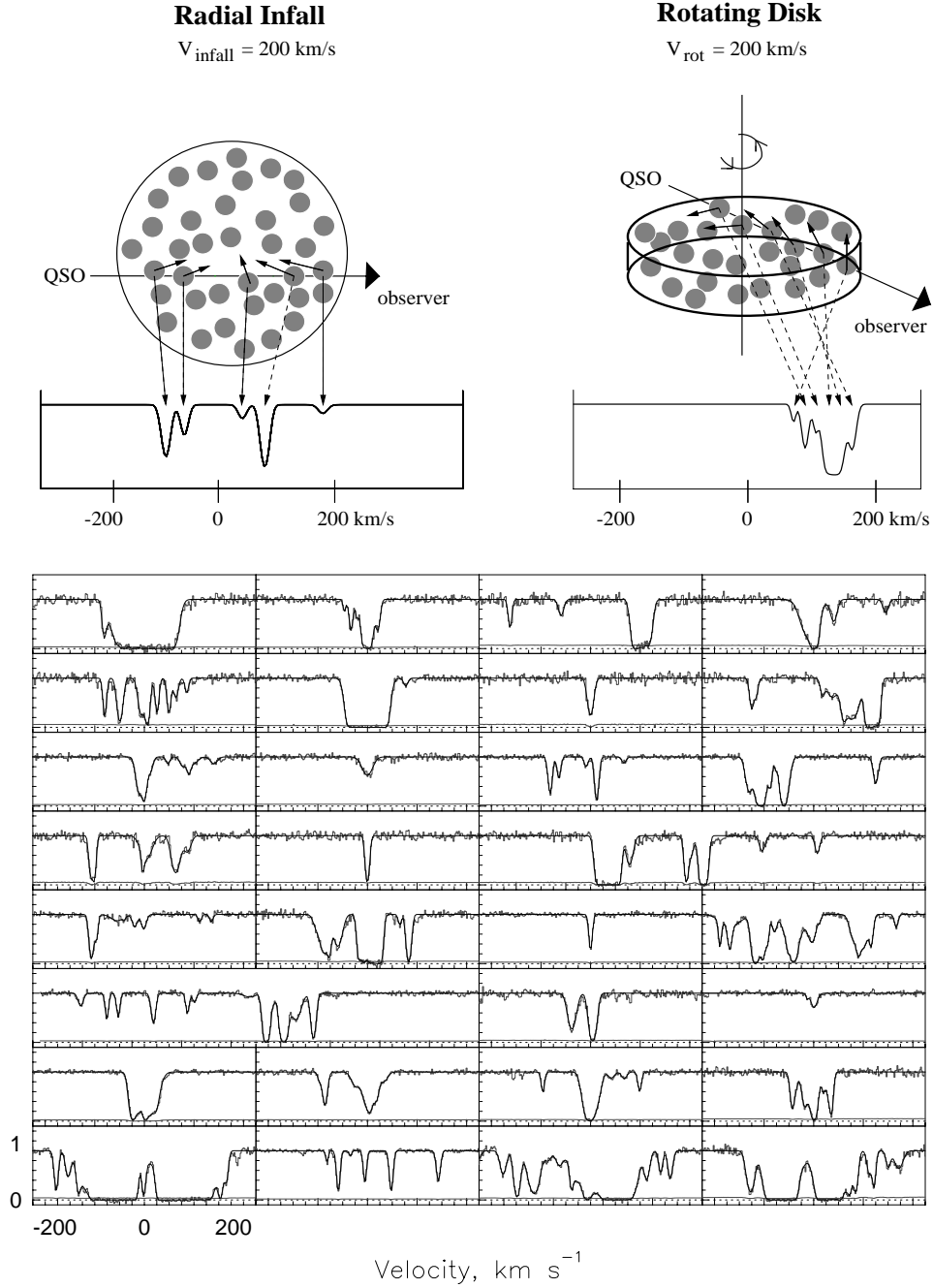


Fig. 5.— Illustrations of two simple kinematic models are shown in the top panel. To the left, the model is radial infall of clouds to the center of a sphere, with constant velocity. The line of sight passes through five clouds, which leads to five different absorption features (for a single transition) in the quasar spectrum. Two of the features are blueshifted relative to the standard of rest of the absorbing galaxy, and the other three are redshifted. The absorption features from a radial infall model can be spread over a velocity of 100–200 km s<sup>-1</sup>, typical of the velocity dispersion of a galaxy halo. To the right, a rotating disk model is illustrated. In this case all the “clouds” along the line of site have a component of motion that is redshifted, and they tend to be clustered together in velocity space, with typical spread of 20–60 km s<sup>-1</sup>. The lower panel shows a sample of  $0.4 < z < 1.4$  MgII absorption profiles observed with the Keck/HIRES spectrograph at  $R = 45,000$ , corresponding to a resolution of  $\sim 6$  km s<sup>-1</sup>. The solid lines through these data are Voigt profile fits and the ticks drawn above the spectrum represent the cloud velocities. Some of these profiles are consistent with the kinematics of a rotating disk, and others with radial infall kinematics. However, to explain the full ensemble of profiles a model combining these two basic types of kinematics is needed.



uniformly throughout the simulation box and photoionization models used to predict the absorption expected from different structures. This is especially important for establishing the kinematics that would be observed from the process of structure formation at high redshifts.

### 3.2. Photoionization Models

Consider a cloud of material, modeled by a plane parallel slab with a certain total column density of Hydrogen,  $N(H) = N(\text{HI}) + N(\text{HII})$ , and with a constant total number density  $n_H = n(\text{HI}) + n(\text{HII})$  along the line of sight. The cloud is also characterized by its metallicity,  $Z$ , which is the ratio of Fe/H expressed relative to the solar value,  $Z_{\odot}$ , and by an abundance pattern (the abundance ratios of all other elements to Fe). The degree of ionization in the gas depends upon the intensity and shape of the spectrum of ionizing radiation. The intensity is characterized by the ionization parameter,  $U = n_{\gamma}/n_H$ , which is the ratio of the number density of photons at the Lyman edge to the number density of Hydrogen ( $n_H = n_e$ , where  $n_e$  is the total number density of electrons). The larger the value of  $U$ , the more ionized the gas. Collisional ionization can also be an important process for some absorption systems with gas at high temperatures (hundreds of thousands of degrees). Photoionization equilibrium models typically yield temperatures of tens of thousands of degrees.

Once the metallicity, abundance pattern, ionization parameter, and spectral shape are specified the equations of radiative transfer can be solved to find the column densities of all the different ionization states of various chemical elements. Figure 6 illustrates, for  $N(\text{HI}) = 10^{16}$  and  $10^{19} \text{ cm}^{-2}$ , the dependence of column densities of various transitions on the ionization parameter,  $U$ . For optically thin gas [ $N(\text{HI}) < 10^{17.2} \text{ cm}^{-2}$ ], the column density ratios of the various metal transitions are not dependent on the overall metallicity, i.e. the curves shift vertically in proportion to  $Z$ . For optically thick gas,

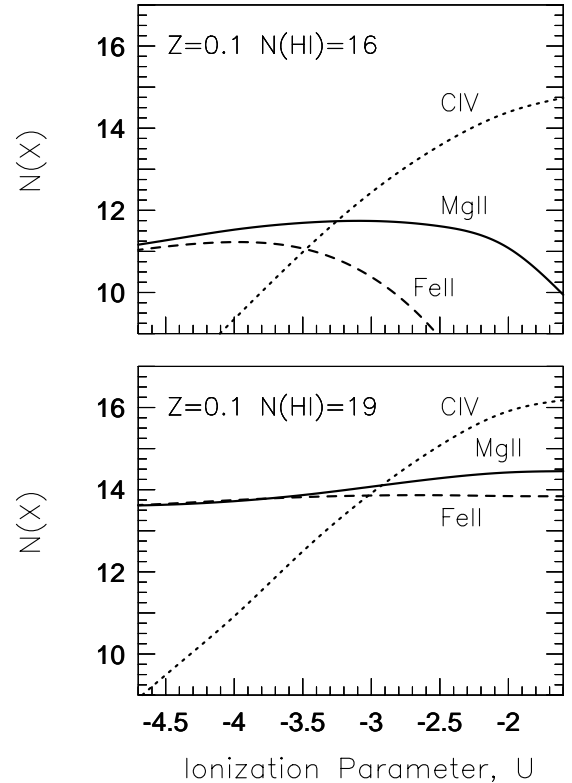


Fig. 6.— Photoionization model predictions of the column densities of MgII, FeII, and CIV as a function of the ionization parameter (the ratio of ionizing photons to the electron number density in the gas). The spectrum incident on the cloud, represented by a constant density slab, is the “Haardt–Madau” spectrum (attenuated spectrum due to integrated effect of quasars and young galaxies). The predicted column densities are presented in two series of models with  $N(\text{HI}) = 10^{16} \text{ cm}^{-2}$  and with  $N(\text{HI}) = 10^{19} \text{ cm}^{-2}$ , the optically thin and optically thick cases. For both, the metallicity is fixed at 10% of the solar value. For the optically thin case, the column densities scale with metallicity, i.e. the ratios remain constant, but for the optically thick case the situation is more complex.

ionization structure develops, with an outer ionized layer around a neutral core, and there is no simple scaling relation with metallicity.

In practice, if we assume that a cloud has a simple, single phase structure, the ratios of the column densities can be used to infer the ionization parameter, which relates to the density of the gas. However, the abundance pattern can differ from the solar abundance pattern because of differing degrees of depletion onto dust, or because of different processing histories. Most of the so-called  $\alpha$  particle nuclei (such as Mg and Si) are synthesized primarily by Type II supernovae during the early history of a galaxy when most massive stars form and quickly evolve to reach their end states. On the other hand, the Fe-group elements are primarily produced by Type Ia supernovae, and therefore build up over a longer timescale. In the basic picture of galaxy evolution, the halo stars are formed early, have been enriched only by Type II supernova, and therefore are  $\alpha$ -element enhanced. Younger disk stars have incorporated also the Type Ia processed material and therefore have relatively larger Fe-group abundances. Ideally, several different ionization states of the same chemical element are observed so that there is no ambiguity between the ionization parameter and the abundance pattern, but this has generally not yet been possible because of limited wavelength coverage at high resolution.

Examples of the variation of column density ratios with velocity in two absorption systems are shown in Figures 7 and 8. In Figure 7,  $N(\text{FeII})/N(\text{MgII})$  varies by an order of magnitude over the four components in the  $z = 1.325$  system toward the quasar Q0117+213. This represents a variation of an order of magnitude in the ionization parameter ( $10^{-4} < U < 10^{-3}$ ), or an order of magnitude variation in the abundance pattern. Figure 8 is a very unusual system with two clouds separated by only  $20 \text{ km s}^{-1}$  in velocity, one of which has a Silicon to Aluminum ratio similar to the Milky Way ISM, and the other

which requires a significant enhancement of Aluminum.

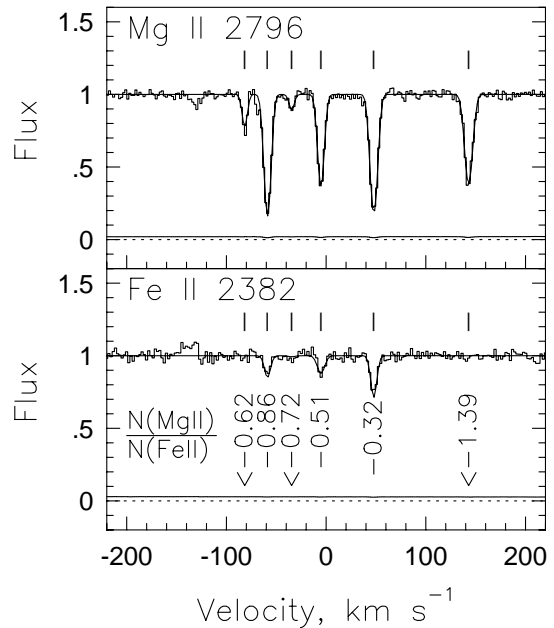


Fig. 7.— Hires/Keck FeII and MgII absorption profiles for the  $z = 1.325$  system in the spectrum of the quasar Q0117+213. The six clouds in this system show a range of more than an order of magnitude in  $N(\text{FeII})/N(\text{MgII})$ , given below each cloud in the lower panel. These variations could be due to cloud to cloud variations of ionization parameter (density) or of abundance pattern within the system.

#### 4. Multiphase Conditions

The gaseous component of the the Milky Way and nearby galaxies have phase structure (i.e. spatial locations with different densities and/or temperatures). Examples are the disk/halo interface (Galactic coronae) and the cold, warm, and hot phases of the interstellar medium. From photoionization models, it is not usually possible to generate absorption that is simultaneously consistent with all observed chemical transitions for a given system. For example, in single cloud MgII systems, Figure 6 (with  $N(\text{HI}) = 10^{16} \text{ cm}^{-2}$ ) shows that if FeII is detected at a similar column density to MgII, the ionization parameter must

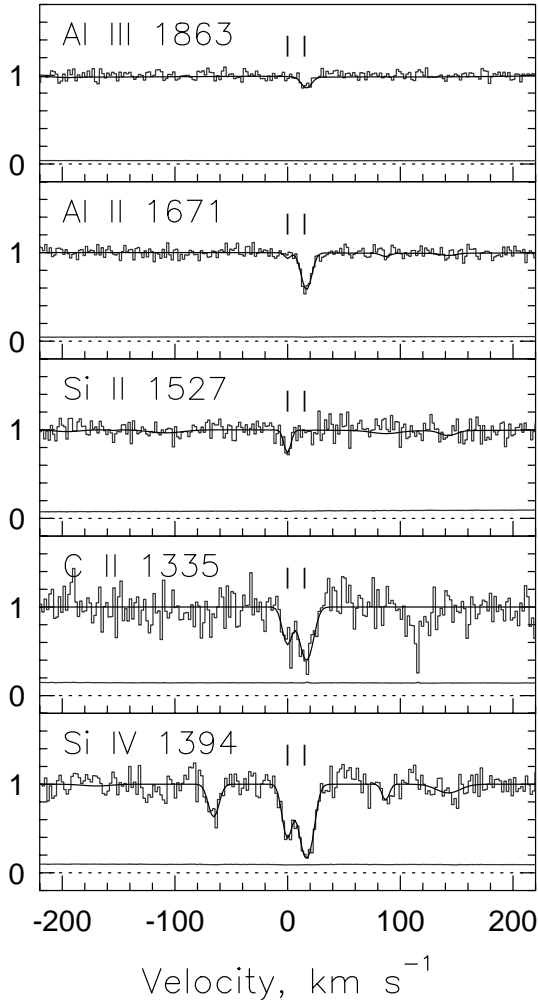


Fig. 8.— An unusual Aluminum-rich cloud is apparent in the  $z = 1.93$  system toward the quasar Q1222+228, and it is close in velocity space to a normal (relative to Galactic clouds) cloud which has detected SiII. Note the different kinematic structure in the higher ionization transitions. The excess of AlII and AlIII in the cloud at  $v = 9 \text{ km s}^{-1}$  is best explained by an abundance pattern variation, since SiII and AlII are transitions with very similar ionization states.

be small, and  $W_r(\text{CIV})$  cannot be large. Many systems have CIV absorption which exceeds this limit and requires a higher ionization (lower density) phase; generally, this phase must have structure over a large velocity range (a large “effective” Doppler parameter). The  $z = 0.93$  system toward the quasar PG 1206+459 is another case that requires multiphase structure. The observed CIV profile in Figure 4 is much too strong for this absorption to arise in the same clouds that produce the MgII, even if their ionization parameters are pushed to the largest values consistent with the data.

## 5. Statistics, Evolution, and Interpretation

Future quasar absorption line studies will combine insights gained from detailed analyses of individual systems with conclusions drawn from the large statistical samples assembled over cosmic time. Evolution of the ensemble of absorption profiles generated by the universal collective of intervening structures is a result of the combined effects of numerous processes. These include growth of structure, star formation, morphological evolution of galaxies, galaxy mergers, and changes in the extragalactic background radiation. Here, we summarize the best present statistical data and likely interpretations for the different classes of absorbers. The number of lines per unit redshift for various populations of absorbers is represented by a power law  $dN/dz \propto (1+z)^\gamma$ . For a universe with only the cosmological evolution due to expansion,  $\gamma = 1.0$  for deceleration parameter  $q_0 = 0$  and  $\gamma = 0.5$  for  $q_0 = 0.5$ .

### 5.1. Ly $\alpha$ Forest

The Ly $\alpha$  forest evolves away dramatically from high to low redshift, as is strikingly clear from the spectra of  $z \sim 3$  and  $z \sim 1$  quasars in Figure 9. The evolution of the Ly $\alpha$  lines with  $W_r(\text{Ly}\alpha) > 0.3 \text{ \AA}$  can be characterized by a dou-

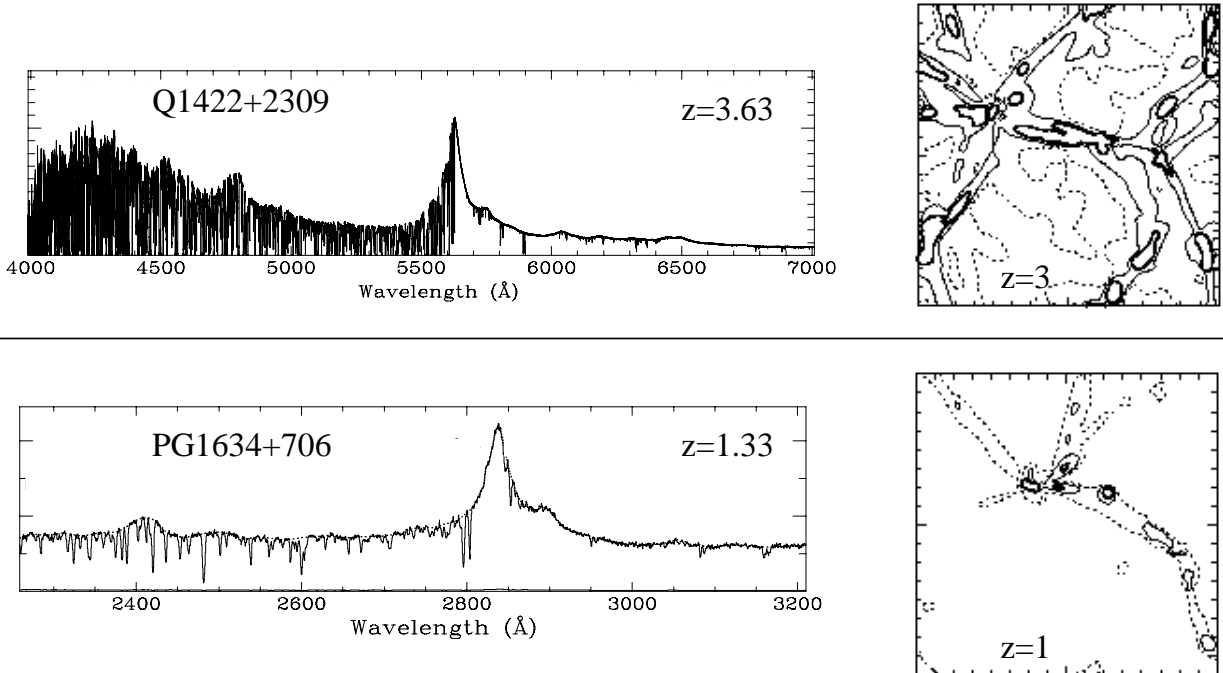


Fig. 9.— Illustration of structure evolution of intergalactic gas from high to low redshift. The upper spectrum of a  $z = 3.6$  quasar is a Keck/HIRES observation, while the lower spectrum is a FOS/HST observations of a  $z = 1.3$  quasar. Higher redshift quasars show a much thicker forest of Ly $\alpha$  lines. Slices through N-body/hydrodynamic simulation results at the two epochs  $z = 3$  and  $z = 1$  are shown in the right-hand panels. Three contour levels are shown:  $10^{11} \text{ cm}^{-2}$  (dotted lines),  $10^{12} \text{ cm}^{-2}$  (solid lines) and  $10^{13} \text{ cm}^{-2}$  (thick solid lines). Evolution proceeds so that the voids become more empty so that even the low column density material is found in filamentary structures at low redshifts.

ble power law with  $\gamma \sim 2$  for  $1.8 < z < 4.5$  and  $\gamma \sim 0.2$  for  $z < 1.8$ . Help in understanding the physical picture has come from sophisticated N-body/hydrodynamic simulations that incorporate the gas physics and consider cosmological expansion of the simulation box. The dynamical evolution of the HI gas can be described as outflow from the centers of voids to their surrounding shells, and flows along these sheets toward their intersections where the densest structures form. This picture is consistent with observational determinations of the “sizes” of Ly $\alpha$  structures. It is difficult to obtain direct measurements of sizes except in some special cases to use “double lines of sight”, close quasar pairs, either physical or apparent due to gravitational lensing. If the spectra of the two quasars both have a Ly $\alpha$  absorption line at the same wave-

length that implies a “structure” which covers both lines of sight. From these studies, it is found that “structures” are at least hundreds of kpc in extent.

At redshifts  $z = 5$  to  $z = 2$   $dN/dz$  for Ly $\alpha$  forest absorption is quite large, but it is declining very rapidly over that range. This dramatic evolution in the number of forest clouds is mostly due to the expansion of the universe, with a modest contribution from structure growth. At  $z < 2$ , the extragalactic background radiation field is falling, and Ly $\alpha$  structures are becoming more neutral. Therefore, the more numerous, smaller  $N(H)$  structures are observed at a larger  $N(HI)$  and this will counteract the effect of expansion, thus slowing the decline of the forest.

The high redshift Ly $\alpha$  forest was once thought

to be primordial material, but in fact it is observed to have a metallicity of 0.1% solar, even at  $z = 3$ . For  $N(\text{HI}) < 10^{14} \text{ cm}^{-2}$ , the expected  $N(\text{CIV})$  would be below the detection thresholds of current observations, so truly pristine material still eludes us. Perhaps it does not exist. To spread metals all through the intergalactic medium may have required a “pre-galactic” population of stars at  $z > 10$  that polluted all of intergalactic space.

## 5.2. Lyman Limit and Metal Line Systems

The  $dN/dz$  of Lyman limit systems is consistent with that of strong MgII absorbers [with  $W_r(\text{MgII}) > 0.3 \text{ \AA}$ ] over the redshift range for which both have been observed,  $0.4 < z < 2.2$ . For  $W_r(\text{MgII}) > 0.3 \text{ \AA}$ ,  $\gamma = 1.0 \pm 0.1$ , consistent with no evolution. For even stronger MgII systems [ $W_r(\text{MgII}) > 1 \text{ \AA}$ ],  $dN/dz$  increases more dramatically with  $z$ , with  $\gamma = 2.3 \pm 1.0$ .

The number of MgII systems (equivalent width distribution) continues to increase down to the sensitivity of the best surveys,  $W_r(\text{MgII}) > 0.02 \text{ \AA}$ , such that  $dN/dz = 2.7 \pm 0.15$  at  $z \sim 1$ . The “weak” MgII absorbers are therefore more common than the strong systems [ $W_r(\text{MgII}) > 0.3 \text{ \AA}$ ] known to be associated with luminous galaxies. Unlike the strong MgII absorbers, the weak MgII absorbers are sub-Lyman limit systems (they do not have Lyman limit breaks), and no galaxies have been identified at the redshift of absorption. Yet, photoionization models indicate that the metallicities of these weak absorbers are at least 10% of the solar value, and in some cases comparable to solar. They are a varied population: some have relatively strong FeII while others have no FeII detected, and some have strong CIV that requires a separate phase while others have no CIV detected. Those with strong FeII are constrained to be smaller than 10 pc (the ionization parameter must be small and  $n_e$  large as can be seen in Figure 6). Also, since Fe is produced primarily by Type Ia supernovae they

must be enriched by a relatively old stellar population. Those with weaker or undetected FeII could be larger (kpcs or tens of kpcs) and possibly enriched by Type II supernovae. Candidate environments that could be traced by weak MgII absorption are: remnants of pre-galactic star clusters formed in mini-halos at  $z > 10$ , super star clusters formed in interactions, tidally stripped material, low surface brightness galaxies, and ejected or infalling clouds (analogous to the Milky Way high velocity clouds).

The evolution of  $dN/dz$  for CIV absorbers can be studied in the optical for high redshifts. For  $W(\text{CIV}) > 0.4 \text{ \AA}$  and  $z > 1.2$ , the number decreases with increasing  $z$ , as  $\gamma = -2.4 \pm 0.8$ . In this same interval, the number of Lyman limit systems is still increasing with redshift, with  $\gamma = 1.5 \pm 0.4$ . This implies that the dramatic evolution in the number of CIV systems is either due to a change in metallicity or a change in ionization state. The  $dN/dz$  for CIV systems peaks at intermediate  $z$  and declines, consistent with no evolution until the present. Combining optical and UV data, CIV and MgII have been compared at  $0.4 < z < 2.2$ . The fraction of systems with large  $W_r(\text{CIV})/W_r(\text{MgII})$  decreases rapidly with decreasing redshift; there is a shift toward “lower ionization systems”.

It is important to consider that the HI, MgII, and CIV absorption do not always arise in the same phase. It is possible that the CIV in many  $z \sim 1$  MgII absorption systems arises in a phase similar to the Galactic coronae. If the origin of this phase is related to star-forming processes in the disk, then it might be expected to diminish below  $z = 1.2$  since the peak star formation rate is passed.

Another important trend is the fact that the very strongest MgII absorbers evolve away from  $z = 2$  until the present. If we study the kinematic structure of these objects, we find that they commonly have a “double” structure, with two separate kinematic regions in the MgII profile. These objects also have strong CIV which also has sepa-

rate components around the two MgII regions in the “double” structure. The CIV does not arise primarily in the individual MgII clouds, nor is it in a smooth, “common halo” structure that extends in velocity space around the entire MgII profile. As more data are collected on the kinematic structure of various transitions in these “double” systems, it will be interesting to consider the hypothesis that galaxy pairs in the process of merger are responsible. The number of these is thought to have been dramatically larger in the past.

### 5.3. Damped Ly $\alpha$ Systems

The  $N(\text{HI}) > 10^{20.3} \text{ cm}^{-2}$  systems are of particular interest because it is possible to observe many different chemical elements (such as Zn, Cr, Fe, Mn, and Ni) in these objects back to high redshift. Metallicities and abundance patterns can be studied and compared to those of old stellar populations in the Milky Way. Back to  $z = 3$ , the metallicity in DLAs, as measured by the undepleted element Zinc, is about 10% of the solar value, but it may decline at  $z > 3$ . The identity of sites responsible for DLAs at high  $z$  remains controversial, but they do contain most of the neutral Hydrogen in the universe, from which most of its stars form. The kinematic structure of the absorption profiles of neutral and low ionization species is consistent with the rotation of a thick disk, so that it is possible that these are the  $z = 3$  progenitors of normal spiral galaxies. However, this signature is not unique. It could also be the consequence of directed infall in an hierarchical structure formation scenario. The higher ionization species show complex kinematics which vary in relation to those of the lower ionization gas; in some systems they appear to trace relatively similar structure, and in others there are clearly several different phases.

At low redshift, many of the galaxies that are responsible for the DLA absorption can be directly identified. These galaxies are a heterogeneous population. They are not just the most lu-

minous galaxies, but include dwarf and low surface brightness galaxies, and even cases where no galaxy has been identified to sensitive limits. Damped Ly $\alpha$  absorption does not trace the most luminous objects, but rather it traces the largest neutral gas reservoirs. An additional selection effect may be important. The most dust-rich galaxies that have the potential to produce DLA absorption could produce enough extinction that their background quasars will not be included in quasar surveys. In this way, the population of DLAs that are actually observed could be significantly biased against dusty galaxy hosts.

## 6. Future Prospects

The next decade will see the synthesis of the various techniques for the study of galaxy evolution, through their stars and through their gas. Higher resolution quasar spectra will be obtained in the ultraviolet (with the Space Telescope Imaging Spectrograph (STIS) and with the Cosmic Origins Spectrograph (COS) on the HST, and later, hopefully, with a larger UV space telescope). It will then be possible to conduct a systematic analysis of the relationships between the different ionization species that trace the different phases of gas in  $0.4 < z < 1.5$  galaxies. In this redshift regime, comparisons to the detailed morphological structure and orientations of the absorbing galaxies is possible from HST images.

Invaluable insights into the origin of quasar absorption lines have been gleaned from absorption studies of nearby galaxies, for which it is possible to directly observe the processes that are involved. Making more observations of this type will be possible by discoveries of bright quasars that fall behind nearby galaxies. The discoveries of quasars in large surveys will also include multiple lines of sight behind distant absorption line systems which can be used to produce 3-D maps of the structures.

The interstellar medium of the Milky Way shows structure on sub-pc scales, and absorp-

tion features can only be resolved with resolution  $< 1 \text{ km s}^{-1}$ . Such a resolution will soon be available on 8m-class telescopes. This is important for separating blends and for looking for metallicity, ionization, and abundance pattern gradients along the line of sight.

The key low ionization transitions of MgII and FeII are shifted into the near-IR region of the spectrum for  $z > 2.5$ . Very soon, near-IR quasar spectra will be obtained at relatively high resolution ( $\sim 20 \text{ km s}^{-1}$ ). Also, IR-imaging, narrow-band techniques, and multi-object spectroscopy in the near-IR should provide much more information about absorbing galaxies at higher redshifts. This will extend evolutionary studies back to an epoch at which formation processes may be contributing significantly to evolution.

## 7. Bibliography

Articles in review journals:

Rauch M 1998 The Lyman Alpha Forest in the Spectra of QSOs *ARAA* **36** 267

Churchill C W and Charlton J C 2000 MgII Absorbers: A Review *PASP* in press

Conference proceedings:

Blades J C, Turnshek D A, and Norman C 1988 *QSO Absorption Lines: Probing the Universe, Proceedings of the QSO Absorption Line Meeting, Baltimore 1987* (Cambridge: Cambridge University Press)

Meylan G 1995 *QSO Absorption Lines: Proceedings of the ESO Workshop, Munich 1994* (Berlin: Springer)

Petitjean P and Charlot S 1997 *Structure and Evolution of the Intergalactic Medium from QSO Absorption Lines* (Paris: Editions Frontières)